Gap solitons under competing local and nonlocal nonlinearities

Kuan-Hsien Kuo,[1] YuanYao Lin,[1] Ray-Kuang Lee,[1] and Boris A. Malomed[2]
[1]*Institute of Photonics Technologies, National Tsing-Hua University, Hsinchu 300, Taiwan*
[2]*Department of Physical Electronics, School of Electrical Engineering, Faculty of Engineering, Tel Aviv University, Tel Aviv 69978, Israel*
(Received 20 December 2010; published 27 May 2011)

We analyze the existence, bifurcations, and shape transformations of one-dimensional gap solitons (GSs) in the first finite band gap induced by a periodic potential built into materials with local self-focusing and nonlocal self-defocusing nonlinearities. Originally stable on-site GS modes become unstable near the upper edge of the band gap with the introduction of the nonlocal self-defocusing nonlinearity with a small nonlocality radius. Unstable off-site GSs bifurcate into a new branch featuring single-humped, double-humped, and flat-top modes due to the competition between local and nonlocal nonlinearities. The mechanism underlying the complex bifurcation pattern and cutoff effects (termination of some bifurcation branches) is illustrated in terms of the shape transformation under the action of the varying degree of the nonlocality. The results of this work suggest a possibility of optical-signal processing by means of the competing nonlocal and local nonlinearities.

DOI: 10.1103/PhysRevA.83.053838 PACS number(s): 42.65.Tg, 42.65.Sf, 42.70.Qs

I. INTRODUCTION

The concept of photonic crystals (PhCs), i.e., artificial media with a periodic modulation of local optical characteristics, provides ways to tailor the dispersion, diffraction, and routing of electromagnetic waves [1]. As for natural crystals, fundamental characteristics of the PhCs are the band diagrams, which reveal gaps where Bloch waves cannot propagate. In PhCs made of nonlinear materials, self-trapped localized modes in the form of the gap solitons (GSs) may exist, as a result of the interplay of the Kerr-type nonlinearity and periodic structures [2–5]. Unlike spatial bright solitons supported by the balance between the self-focusing nonlinearity and diffraction in uniform bulk media [6], the dispersion relation induced by the PhC makes it possible to create GSs in both focusing and defocusing media. Combining assets of PhCs and regular solitons, GSs have a potential for applications to soliton-driven photonics. New technologies enabling reconfigurable optical lattices, such as photorefractive crystals [7] and nematic liquid crystals [8], also open new ways to control the dynamics of solitary waves by adjusting the lattice depth and period.

While the modulational [9] and oscillatory instabilities [10,11] impose limits on the use of the GSs, the stability and mobility of the GSs may be enhanced in nonlinear media featuring a nonlocal response [12–15]. The nonlocal nonlinearity is important when the correlation radius of the material's response function becomes comparable to the transverse width of the wave packet [16,17]. The nonlocal nonlinearity gives rise to specific features in the soliton dynamics, including the modification of the modulational [18], azimuthal [19], and transverse [20] instabilities. Suppression of the collapse of multidimensional solitons [21], a change of the character of interactions between them [22], formation of soliton bound states [23], merger of colliding solitons into a standing wave [24], and families of dark-bright soliton pairs [25] were also predicted recently. Experimental observations of the nonlocal response have also been demonstrated in sundry media, including photorefractive media [26], nematic liquid crystals [27], and thermo-optical materials [28,29], with a large tunable range of the nonlocality degree.

In this work, we aim to study GS modes in the first band gap of the model, including local self-focusing and nonlocal self-defocusing nonlinearities. When the nonlocality radius is zero, we assume equal magnitudes of the self-focusing and self-defocusing terms, i.e., complete cancellation of the nonlinearity, hence no solutions in the band gap. For a small degree of the nonlocality, the existence, bifurcation, and shape transitions of the emerging bright GSs are analyzed. With the competing local and nonlocal interactions of opposite signs, the family of on-site GS modes remain stable, obeying the "anti-Vakhitov-Kolokolov" criterion [30], for the case where the nonlocal perturbation of the refractive index is small but becomes unstable near the upper edge of the band gap. However, the bifurcation generating the GSs near the other edge of the band gap features an inverted slope of the bifurcation curve for a relatively small degree of the nonlocality, in which case the on-site GSs are unstable. The off-site GS family features single-humped, double-humped, and flat-top profiles for different degrees of the nonlocality. We also investigate the situation in the space of the soliton's propagation constant and power, for the varying nonlocality degree, in order to illustrate the mechanism underlying the complex bifurcation pattern and related cutoff effects (termination of some solution branches). Using results reported in this work, we discuss the possibility to design GS-based signal-processing schemes by dint of manipulating the nonlocal interactions.

In addition to optics, GSs of matter waves have also been theoretically studied [31] and experimentally created [32] in Bose-Einstein condensates (BECs) formed by atoms with repulsive interactions, trapped in optical-lattice (OL) potentials. In addition to the known contact interaction in the BECs of alkali-metal atoms, the interaction of chromium atoms, ^{52}Cr, includes a dipole-dipole interaction, which is intrinsically anisotropic and nonlocal. The condensate of ^{52}Cr was created and investigated using magnetic [33–36] and all-optical [37] traps; see also review [38]. By adjusting the orientation of the dipoles, one can effectively control the nonlocal dipole-dipole interactions. For the dipolar BEC trapped in OLs, the competition between the contact and long-ranged dipole-dipole interactions not only dramatically

change the band structures of nonlinear Bloch waves [39] but also modifies families of matter-wave solitons [40].

The rest of the paper is organized as follows. In Sec. II, the model including the competing local and nonlocal nonlinearities is described. Properties of the on-site and off-site GS families supported by the local self-focusing nonlinearity are recapitulated to show a transition of mode profiles in the first band gap. Results produced by the interplay of the local self-focusing and nonlocal self-defocusing nonlinearities for on-site and off-site GS families are reported in Secs. III and IV, respectively. Tracing the change of the corresponding GS shapes in the parameter planes, we explain the character of the corresponding bifurcation and identify a possible control mechanism for the optical-signal processing. Section V concludes this work.

II. THE GAP-SOLITON FAMILY WITH THE LOCAL SELF-FOCUSING NONLINEARITY

Considering a wave packet propagating along the η axis in the nonlinear PhC structure, we assume that the embedded medium gives rise to two kinds of the nonlinearity simultaneously. This system is modeled by the modified nonlinear Schrödinger equation [15],

$$i\frac{\partial\Psi}{\partial\eta} = -\frac{1}{2}\frac{\partial^2}{\partial\xi^2}\Psi + V(\xi)\Psi + \sigma n(\xi)\Psi + \rho|\Psi|^2\Psi, \tag{1}$$

$$n - d\frac{\partial^2 n}{\partial\xi^2} = |\Psi|^2, \tag{2}$$

where $\Psi(\eta,\xi)$ is the slowly varying amplitude of the electric field and $V(\xi)$ is the periodic potential, and a perturbation of the refractive index, $n(\xi)$, accounts for the diffusive nonlinear response with the nonlocality degree (which scales as a squared nonlocality radius) designated by parameter d. Sign parameters $\sigma,\rho = +1$ and -1 correspond to the self-defocusing and self-focusing nonlinearities, respectively. Below, we fix $\sigma = +1$ and $\rho = -1$ for a system with the nonlocal self-defocusing and local self-focusing nonlinearities.

Stationary solutions with propagation constant $-\mu$ are looked for as $\Psi(\eta,\xi) = \Phi(\xi)e^{-i\mu\eta}$. For periodic potential $V(\xi) = 4\sin^2(k_0x)$ with $k_0 = 1$ fixed by rescaling, the linearized version of Eq. (1) gives rise to the band-gap structure, with the first finite band gap being $1.3047 < \mu < 3.1896$. In this band gap, GSs can exist in form of on-site and off-site modes being supported solely by the local nonlinearity, i.e., with $\sigma = 0$ [9]. For the self-focusing Kerr nonlinearity, we display examples of both the on-site and off-site GS solutions in Fig. 1. The relationships between μ and the power of these modes, $P = \int_{\infty}^{\infty} d\xi|\Phi|^2$, are shown in the form of the bifurcation curves in Fig. 1(g), with labels A through F referring to typical GS mode profiles in subplots (a)–(f).

Under the self-focusing nonlinearity, these GSs bifurcate from the upper edge of the first band gap (in other words, from the lower edge of the second finite Bloch band), where the spatial-dispersion law features the anomalous sign [41]. In the entire first band gap, the odd on-site GS modes, shown in Figs. 1(a)–1(c), feature two major peaks within one lattice cell. Tails of these modes become conspicuous

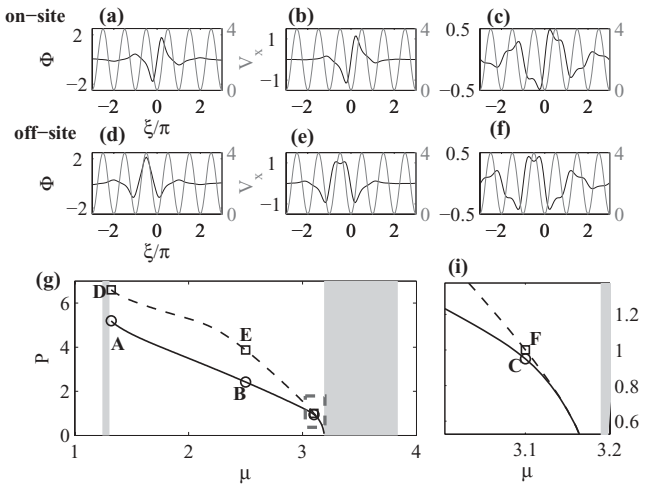

FIG. 1. Examples of on-site [(a)–(c)] and off-site [(d)–(f)] gap-soliton solutions and the corresponding potential V in the case of the local self-focusing Kerr nonlinearity, depicted by black and gray lines, respectively. The propagation constant of each mode is indicated by labels A through F in panel (g), where the relations between the propagation constant and power are plotted by the solid and dashed curves, respectively, for the on-site and off-site modes. Panel (i) shows a close-up of the area enclosed by the dashed box in (g). Here and in other figures, shaded areas represent Bloch bands bordering the first finite band gap.

when the propagation constant moves close to the upper edge of the band gap. On the other hand, a shape transition is demonstrated by the off-site even GS modes. Near the lower edge of the band gap, the GS solution has a single major peak coinciding with a local maximum of the periodic potential, as shown in Fig. 1(d). By tracing the variation of the propagation constant and power along the relation for these off-site modes shown by the dashed line of Fig. 1(g) to point F, it is seen in Fig. 1(f) that the center of the modal profile breaks into two peaks. The double-peaked solution is formed due to the balance between the repulsive potential barrier and self-trapping induced by the Kerr nonlinearity, as the characteristic self-trapping length becomes larger than a half of the lattice period (roughly equivalent to the width of the barrier potential). In between, we observe a smooth shape transition of the GS from the single-humped shape in Fig. 1(d) to a nearly flat-top one in Fig. 1(e), and, finally to the double-peaked mode in Fig. 1(f).

The off-site GSs exist when the nonlinear self-trapping is stronger than the repulsion induced by the potential barrier, giving rise to an effective a potential well holding the localized modes, as seen in Figs. 1(d)–1(f). On the other hand, the effect of the lattice potential is stronger than that of the nonlinearity in the case of the on-site modes, which, together with the contribution of the gradient energy, determines their shapes in Figs. 1(a)–1(c). When the refractive index correction gets weaker in accordance with the power reduction, the concave lattice potential create a potential barrier to tailor and split the wave function into a form of the states that similar to a binding profile from two on-site modes in Fig. 1(b).

III. ON-SITE GAP SOLITONS UNDER COMPETING LOCAL AND NONLOCAL NONLINEARITIES

In this section, we introduce the self-defocusing nonlocal nonlinearity, setting $\sigma = 1$ in Eq. (1). Obviously, in this case the total nonlinearity cancels out to zero in the limit of $d = 0$. At $d > 0$, the overall nonlinearity is self-focusing, because the diffusive nonlocal kernel produces a spatially wider and less intensive perturbation of the nonlinear refractive index, in comparison with that corresponding to the local nonlinearity. Then, similarly to the situation in the linear model outlined above, one may expect the corresponding GS modes to bifurcate from the upper edge of the first band gap, where the effective spatial dispersion is anomalous. In Fig. 2, we show examples of on-site GSs supported by the competing local focusing and nonlocal defocusing nonlinearities for different degrees of nonlocality, $d = 0.1,1,40$, and the case of $\rho = 0$ (the local nonlinearity only) for the comparison.

For different degrees of the nonlocality, the profiles of the on-site GS solutions vary slightly, remaining similar to their counterparts in the local model. On the other hand, Fig. 2(f) demonstrates that the power required for the formation of the GSs is higher in the model with the competing nonlinearities than in the local one because the net nonlinearity is effectively reduced by the competition of the nonlocal nonlinear response with the local Kerr term. In the limit of the ultimate nonlocality, $d \to \infty$, the $P(\mu)$ curve converges to that in the local model (with $\rho = 0$). The latter feature is explained by the fact that, in this limit (which corresponds to the model of the so-called "accessible solitons" [16]), the nonlocal nonlinear response amounts to a weak constant background, which shifts the propagation constant by the amount proportional to $P/\sqrt{d}$ [15].

In Fig. 2(f), the bifurcation curve shows an abrupt change of the slope both for $d = 1$ and $d = 0.1$ (in the latter case, near point E). In a small region to the left of this

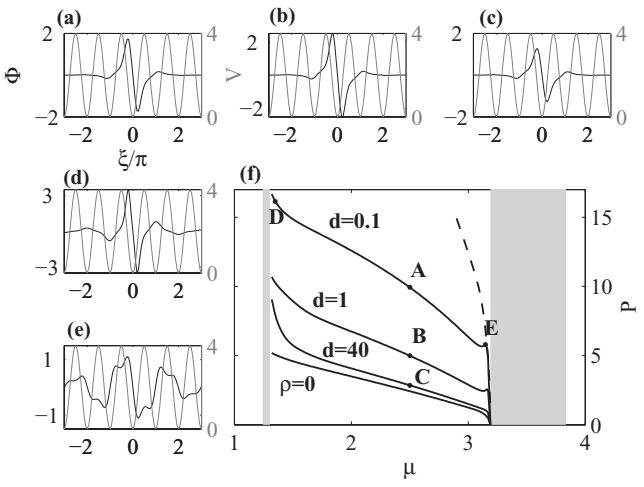

FIG. 2. Examples of on-site [(a)–(e)] gap solitons in the case of the competing local and nonlocal nonlinearities (black lines) and the corresponding potential V (gray lines) for different degrees of the nonlocality $d = 0.1,1,40$, and the case of $\rho = 0$ (local only). The corresponding values of propagation constant μ are labeled (A)–(E) in panel (f). The dashed line in (f) is the asymptotic curve for $d = 0.1$.

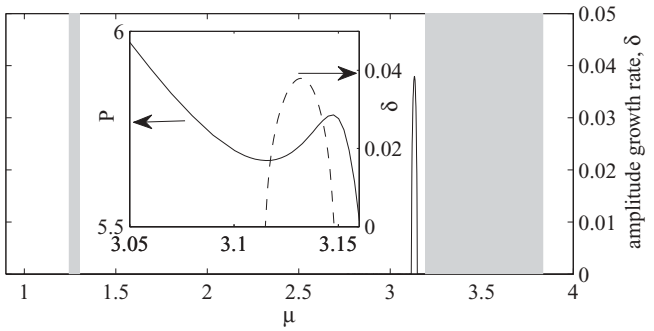

FIG. 3. Amplitude growth rate of small-perturbation modes on the gap solitons in the case of the competing local and nonlocal nonlinearities for the degrees of the nonlocality $d = 0.1$. The inset shows the close-up of stability analysis along with the corresponding power-propagation constant relations.

point, the slope changes its sign to $d\mu/dP > 0$, and the corresponding on-site GSs are unstable. It is known that the bifurcation curves for GS families supported by the local self-focusing nonlinearity obeys an inverted "anti-Vakhitov-Kolokolov" criterion [9], $d\mu/dP < 0$, under which the on-site GSs are stable (see also Ref. [30]). To elucidate, we analyzed the stability of the numerically found GS families by considering small-perturbation modes and calculating their eigenvalues. Specifically, we show in Fig. 3 the linear stability analysis spectrum over the entire first band-gap regime. It is clearly illustrated in the inset of Fig. 3, unstable small-perturbation eigenmodes are obtained only within the region where the power dependence $d\mu/dP > 0$ and therefore confirms the inverted "anti-Vakhitov-Kolokolov" criterion. The evolution of these on-site gap solitons generated by direct numerical simulations further shows the collapse of on-site solitons falling out of the "anti-Vakhitov-Kolokolov" regime.

When the propagation constant of the GS is close to the upper edge of the band gap (on the right-hand side of the slope-change point), the slope of the $P(\mu)$ becomes negative again. In that case, the GS is broad, spanning a few lattice periods, and resembles *gap wave* modes [31], as seen in Fig. 2(e). The abrupt slope change smooths out with the increase of the nonlocality degree, disappearing at $d \simeq 5$, due to the fact that the nonlocal perturbation of the refractive index becomes small for the strong nonlocality.

For a sufficiently small degree of the nonlocality, d, Fig. 2 shows that the power required to form the GSs increases with the decrease of d, diverging at $d \to 0$. In the regime of the weak nonlocality, the effective competing nonlinearity can be approximated, to the first order in d, as [25] $n(\xi)|\Psi|^2 - |\Psi|^2\Psi \approx d\left(|\Psi|^2\right)_{\xi\xi}$, which implies that the soliton's power scales as $1/d$. An asymptotic curve based on this approximation is shown by the dashed line in Fig. 2(f) to illustrate the bifurcation of the on-site GSs near the upper edge of the first band gap.

IV. OFF-SITE GAP SOLITONS UNDER COMPETING LOCAL AND NONLOCAL NONLINEARITIES

Next, we aim to study off-site GSs in the first finite band gap under the action of the competing nonlinearities. As mentioned

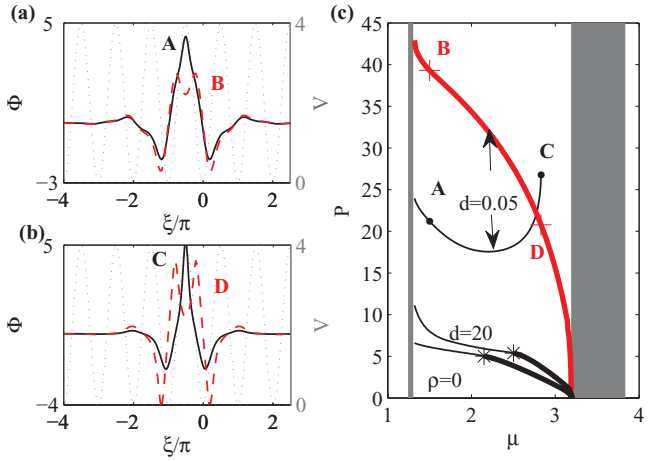

FIG. 4. (Color online) Off-site gap solitons in the model with the competing local self-focusing and nonlocal self-defocusing nonlinearities for the points marked in panel (c): A and B (a) and C and D (b). The bifurcation curves for two very different values of the degree of the nonlocality, $d = 0.05$ and 20, are shown in (c) to indicate the cases with and without the new branch. Thin and thick portions of $P(\mu)$ curves pertain to the solitons with single- and double-peak profiles, respectively.

in Sec. II, the profile of the off-site GS solutions changes from single-humped to double-humped as propagation constant μ approaches the upper edge of the band gap. To indicate the change of the profile caused by the introduction of the competing nonlocal nonlinearity, in Fig. 4(c) we use thin and thick lines to distinguish portions of the $P(\mu)$ curves representing such single- and double-humped profiles. Again, in the limit of the strong nonlocality, the correction to the refractive index induced by the nonlocal nonlinearity is widely spread in the space and very small with respect to the effect of the Kerr nonlinearity, which makes the competition negligible. For example, for $d = 20$ [see Fig. 4(c)], both the $P(\mu)$ curve and the corresponding shape transition of the off-site GSs are close to their counterparts in the local model. A smooth transition of the GS solutions from the single-peaked shape to a flat-top one and then to the double-peaked (in-phase) shape can be traced, in the latter case.

However, for a smaller degree of the nonlocality, which makes the self-defocusing nonlocal response comparable to the Kerr nonlinearity, the analysis reveals the existence of more than one branch of the off-site GSs. For small values of d, such as $d = 0.05$ shown in Fig. 4(c), one branch (the bold red curve in the figure) extends continuously from the upper to lower edge of the band gap. The modal profile for this branch remains double humped, such as the one shown by dashed lines of Figs. 4(a) and 4(b) for markers B and D in (c), respectively. Besides this branch of the double-humped GS modes, there is a separate branch representing solutions with a lower formation power and single-humped profile, as shown by solid lines in Figs. 4(a) and 4(b) for markers A and C in panel (c).

Thus, the single- and double-peaked GSs, which constitute parts of the single GS family in the local model, split into two disjoint families in the model with the appreciable competition between the local and nonlocal nonlinearities. In

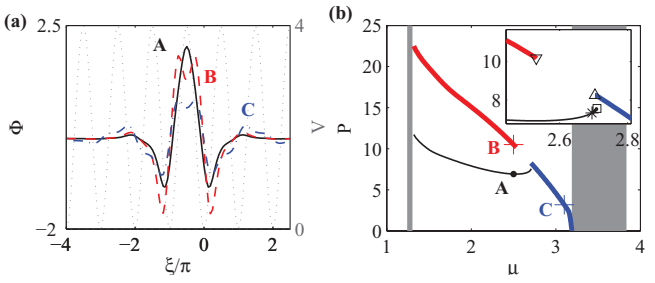

FIG. 5. (Color online) (a) Off-site GSs under the competing local self-focusing and nonlocal self-defocusing nonlinearities, corresponding to the points A, B, and C in panel (b), where the $P(\mu)$ curves for the nonlocality degree $d = 2$ are shown. The thin and thick lines distinguish portions corresponding to single- and double-peaked modes, respectively. The inset in (b) is a close-up of the region around the marked points.

the intermediate case, corresponding to a moderate degree of the nonlocality, such as for $d = 2$ shown in Fig. 5(b), the $P(\mu)$ curve for the double-humped GSs breaks into two segments: one starts from the lower edge of the band gap and ends at a cutoff point corresponding to marker B in the figure, and the other starts from the upper edge and ends at another cutoff point, which is designated by marker $\triangle$. The cutoff points may be accounted for by bifurcations involving additional higher-order modes, which we did not aim to find in this work dealing with fundamental on- and off-site GSs. Another $P(\mu)$ branch chiefly represents the single-humped GSs, but it also contains a portion to the right of point A, which corresponds to double-humped modes.

The inset of Fig. 5(b) clearly shows that there are three branches of double-humped modes. The first one bifurcates from the upper edge of the band gap and ends at the point marked $\triangle$; the second one extends from the lower edge of the band gap and terminates at point labeled by $\triangledown$; the final branch bifurcates as the flat-top solution from the point marked the asterisk ($*$) and terminates at the site marked $\square$. The first two branches that bifurcate from either edge of the band gap abruptly terminate inside the band gap, where the characteristic width of the nonlinear response is larger than or comparable to half the lattice period, which makes the balance between the nonlinear and lattice-induced effects impossible. The last branch, which starts as the flat-top mode, ends due to the divergence of the total power as a result of vanishing nonlinearity, similarly to the cutoff considered in Ref. [42].

Even though off-site GSs are in general unstable both in local [9] and nonlocal [13] nonlinearities despite the inverted "anti-Vakhitov-Kolokolov" criterion, the corresponding instability growth rate is proportional to the GS's power after a certain threshold value [10,13]. Due to the unstable nature of off-site GSs, we study the instability of GSs by the linear stability analysis for the branches off-site GSs and identify the final state of these off-site GSs by beam propagation simulation. The linear stability spectrum in Fig. 6 shows the amplitude growth rate of the small-perturbation eigenmodes found on those off-site GS's revealed previously. For a smaller degree of nonlocality, $d = 0.05$, illustrated in Fig. 6(a), the two distinct branches are unstable and the corresponding eigenmodes on single-peaked GSs have a higher amplitude

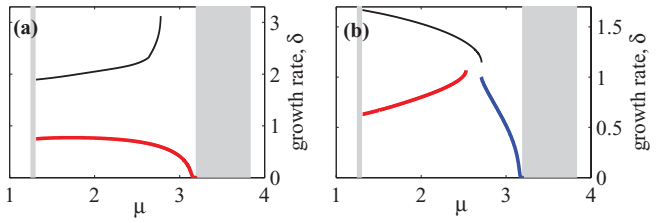

FIG. 6. (Color online) Eigenvalues of small-perturbation mode on the off-site GSs under the competing local self-focusing and nonlocal self-defocusing nonlinearities, of which the degree of nonlocalities are (a) $d = 0.05$ and (b) $d = 2$. The color and line style to distinguish each branch is as is defined in the corresponding $P(\mu)$ curves in Figs. 4(a) and 5(b), respectively.

growth rate which diverges near its cutoff point in the band-gap region. The GSs on these two branches collapse fast as they propagate due to a larger growth rate. Likewise, in Fig. 6(b), when a moderate degree of nonlocality, $d = 2$, is considered, the single-peaked GSs branch acquires a stronger instability than that of the two separated double-peaked GSs branches. The two double-peaked GSs branches, though both feature the worst instability near their cutoff points in the band-gap region, reflect very different relations to the corresponding GS's power, which we believe is stemmed from the cutoff of the branches.

The beam propagation simulations further illustrate that GSs of the single-peaked branch and double-peaked modes with a higher energy fall into collapsed states. Nevertheless, mode conversions from unstable off-site GSs into stable on-site GSs are observed for the branch plotted in blue in Fig. 5(b). Three examples of beam propagation simulations are illustrated, resulting in either collapsed states Figs. 7(a) and 7(b) or a mode conversion behavior; Fig. 7(c). Information such as mode transition or conversion is beyond what linear stability analysis may reveal. Even though it is also believed that interesting dynamical behavior associated with the GSs can be delineated through a direct beam propagation simulation, yet to be more focused, a thorough investigation of propagation behavior goes beyond the scope of this work.

The nonlocal nonlinearity competing with the local Kerr term not only reduces the strength of the nonlinearity but also tailors the effective nonlinear response to induce binding

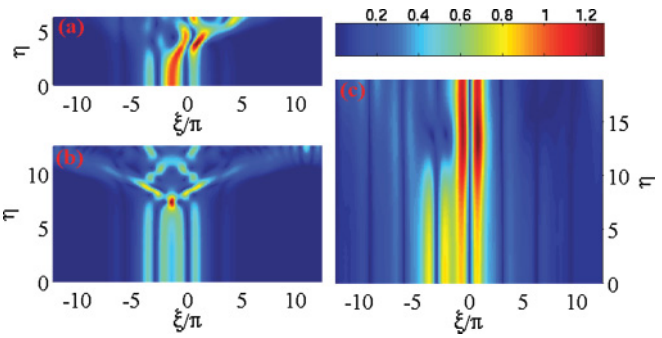

FIG. 7. (Color online) Three examples of the beam propagation simulations for off-site GS solutions shown in Fig. 5(a), in which modes A, B, and C correspond to intensity plots in (a), (b), and (c), respectively.

forces outside the lattice-potential barriers, which is a more favorable environment for the existence of double-peaked modes. Therefore, the three GS branches outlined above are formed due to the interplay of the potential barrier created by the lattice potential and the binding potential induced by the effectively *reduced* Kerr nonlinearity. In this case, the GS solutions belonging to the branch originating from the lower edge of the band gap have a larger amplitude and are more tightly localized. The width of the corresponding response range of the self-defocusing nonlocal nonlinearity is larger than that of the Kerr response. Such a double-peaked branch cannot exist in the strong-nonlocality limit, and we numerically find that values of the nonlinearity degree supporting this branch are bounded by $d < 9.2$. As the power decreases (the propagation constant increases), the widening of the the GS mode makes the overall nonlinear response effectively local, suppressing the capability of the nonlocal nonlinearity to tailor its response to a shape necessary for supporting the solitons. Then, when the GS width becomes smaller than or comparable to half the lattice period, the double-peaked modes cease to exist because the balance between the lattice potential and nonlinearity-induced perturbation of the refractive index supports only single-peaked modes.

To present a clear description of shape transitions for the off-site GSs, we replot the relationship of power P versus the nonlocality degree, d, for a fixed propagation constant μ in Fig. 8. For a smaller propagation constant, such as $\mu = 1.5$ in Fig. 8(a), the power necessary to support a single-humped off-site GS is always lower than that of its double-humped counterpart for all values of d. Moreover, above a critical degree of the nonlocality, $d = 7.3$ in this case, only a single-humped GS can be found. Moving μ into the center of the band gap [for instance, taking $\mu = 2.69$ in Fig. 8(b)] the critical degree of the nonlocality reduces to $d = 1.9$, and, above another critical value, $d = 2.35$, the single-humped

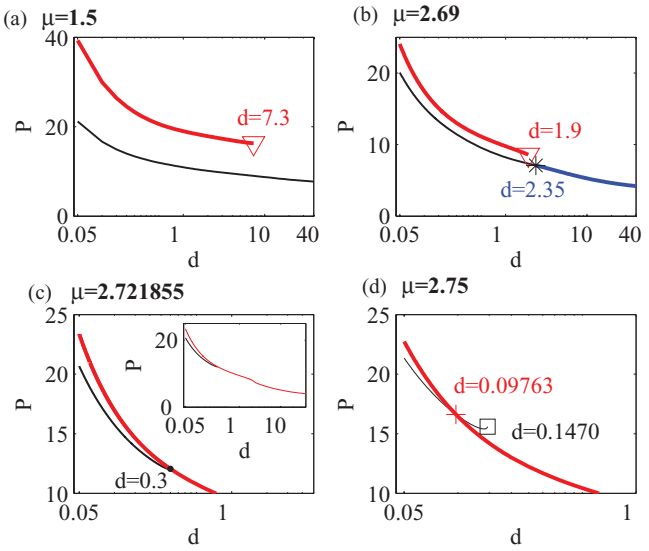

FIG. 8. (Color online) The power, P, versus the degree of the nonlocality, d, at fixed values of the propagation constant: $\mu = 1.5$ (a), 2.69 (b), 2.721855 (c), and 2.75 (d), respectively. The inset in (c) is a close-up of the region in the vicinity of the merger point.

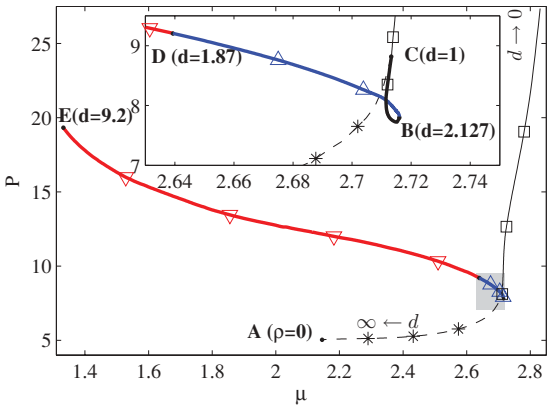

FIG. 9. (Color online) The diagram in the plane of the propagation constant (μ) and power (P), for the gap solitons, as different values of the nonlocality degree, d. The inset is a close-up of the gray region. Route AC corresponds to the transition point marked by $*$ in Fig. 4; routes BC and BDE correspond to the double-peaked modes marked by $\triangle$ and $\triangledown$ in Fig. 5, respectively; the route above point C corresponds to the single-peaked solution. The marked points are A with $\rho = 0$ and B, C, D, and E with $d = 2.127$, 1, 1.86911, and 9.2.

mode transforms into a double-humped one, as in the local model. Increasing the value of the propagation constant to $\mu = 2.721855$, the two $P(d)$ curves merge at $d = 0.3$ in Fig. 8(c). For a larger value of the propagation constant, such as $\mu = 2.75$ in Fig. 8(d), the two curves intersect at a critical value $d = 0.09763$. Above this critical point, the power for the double-humped off-site GS becomes lower than for a single-humped one. In this case, the profile of the off-site GS mode can be switched from single humped into double humped by adjusting the nonlocality degree, d.

To facilitate the understanding of the present picture, we consider the plane of the propagation constant μ and power P for the GS solutions in Fig. 9, varying the nonlocality degree d. We start by tracing the evolution of the point of the transition from single-peaked to the double-peaked shape, marker by the asterisk ($*$) in Fig. 5(c). In the absence of the competing nonlocal nonlinearity, i.e., at $\rho = 0$ in Eq. (1), the transition point is ($\mu = 2.145, P = 5.0460$), labeled by A in Fig. 9, which also corresponds to the limit of $d \to \infty$. As the nonlocality degree drops to a critical value, $d = 1$ at point C ($\mu = 2.7133, P = 8.8184$), the transition point ceases to exist (i.e., only sharply peaked single-humped modes are supported by the system), merging into to the end point of the doubled-humped-mode branch, marked by $\square$ in Fig. 5. Increasing the nonlocality degree from $d = 1$ at point C, the end point $\square$ in Fig. 5 merges into the other end point $\triangle$ in Fig. 5 at $d = 2.127$. The latter merger happens at point B in Fig. 9. This is the end point of the family of the double-peaked modes [an example corresponds to the point marked by $\triangle$ in the inset of Fig. 5 (b)] which originates from point B in Fig. 9 at the critical nonlocality $d = 2.127$ and extends toward point D, which corresponds to $d = 1.86911$, where it merges into a new branch of the double-peaked modes emerging (as long as $d < 9.2$) from the lower edge of the band gap at point ($\mu = 1.3047, P = 19.3262$).

V. CONCLUSION

In this work, we aimed to study GS (gap-soliton) solutions in the first finite band gap of the periodic potential, with the nonlinearity represented by the competing local self-focusing and nonlocal self-defocusing terms. The two terms are balanced so, in the limit of the zero nonlocality radius, they exactly cancel each other. While keeping the effective interaction self-attractive, the existence, stability, and bifurcation for on-site and off-site modes were analyzed numerically. Due to the opposite signs of the local and nonlocal nonlinearities, an increased power was required for the formation of both the on-site and off-site GSs. The competing nonlinearities induce a region where stable on-site modes obeying the "anti-Vakhitov-Kolokolov criterion" near the upper edge of the band-gap region become unstable. For unstable off-site GS modes, which remain unstable under competing local and nonlocal nonlinearities, a complex bifurcation pattern with cutoff points was found and explained in terms of the transitions between the single-humped, flat-top, and double-humped shapes. By tracing the evolution with the change of the nonlocality degree, we have shown that it is possible to switch different off-site GS modes by manipulating the nonlocal interaction against the local Kerr nonlinearity.

ACKNOWLEDGMENT

This work was partly supported by the National Science Council of Taiwan with contracts NSC 95-2112-M-007-058-MY3, NSC 95-2120-M-001-006, and NSC 98-2112-M-007-012.

[1] J. D. Joannopoulos, R. D. Meade, and J. N. Winn, *Photonic Crystals: Molding the Flow of Light* (Princeton University Press, Princeton, NJ, 1995).

[2] *Nonlinear Photonic Crystals*, edited by R. E. Slusher and B. J. Eggleton (Springer-Verlag, Berlin, 2003).

[3] B. J. Eggleton, R. E. Slusher, C. M. de Sterke, P. A. Krug, and J. E. Sipe, Phys. Rev. Lett. **76**, 1627 (1996).

[4] F. Kh. Abdullaev, B. B. Baizakov, S. A. Darmanyan, V. V. Konotop, and M. Salerno, Phys. Rev. A **64**, 043606 (2001); I. Carusotto, D. Embriaco, and G. C. La Rocca, *ibid.* **65**, 053611 (2002); E. A. Ostrovskaya and Yu. S. Kivshar, Phys. Rev. Lett. **90**, 160407 (2003).

[5] V. A. Brazhnyi and V. V. Konotop, Mod. Phys. Lett. B **18**, 627 (2004).

[6] Yu. S. Kivshar and G. P. Agrawal, *Optical Solitons: from Fibers to Photonic Crystals* (Academic Press, San Diego, 2003).

[7] N. K. Efremidis, S. Sears, D. N. Christodoulides, J. W. Fleischer, and M. Segev, Phys. Rev. E **66**, 046602 (2002).

[8] M. Peccianti, K. A. Brzdkiewicz, and G. Assanto, Opt. Lett. **27**, 1460 (2002).

[9] D. E. Pelinovsky, A. A. Sukhorukov, and Yu. S. Kivshar, Phys. Rev. E **70**, 036618 (2004).
[10] B. A. Malomed and R. S. Tasgal, Phys. Rev. E **49**, 5787 (1994).
[11] I. V. Barashenkov, D. E. Pelinovsky, and E. V. Zemlyanaya, Phys. Rev. Lett. **80**, 5117 (1998).
[12] Z. Xu, Y. V. Kartashov, and L. Torner, Phys. Rev. Lett. **95**, 113901 (2005).
[13] Y. Y. Lin, I-H. Chen, and R.-K. Lee, J. Opt. A: Pure Appl. Opt. **10**, 044017 (2008).
[14] Y. Y. Lin, R.-K. Lee, and B. A. Malomed, Phys. Rev. A **80**, 013838 (2009).
[15] Y. Y. Lin, C. P. Jisha, C. J. Jeng, R.-K. Lee, and B. A. Malomed, Phys. Rev. A **81**, 063803 (2010).
[16] A. W. Snyder and D. J. Mitchell, Science **276**, 1538 (1997).
[17] W. Królikowski and O. Bang, Phys. Rev. E **63**, 016610 (2000).
[18] W. Królikowski, O. Bang, N. I. Nikolov, D. Neshev, J. Wyller, J. J. Rasmussen, and D. Edmundson, J. Opt. B **6**, S288 (2004).
[19] S. Lopez-Aguayo, A. S. Desyatnikov, and Yu. S. Kivshar, Opt. Express **14**, 7903 (2006).
[20] Y. Y. Lin, R.-K. Lee, and Yu. S. Kivshar, J. Opt. Soc. Am. B **25**, 576 (2008).
[21] O. Bang, W. Królikowski, J. Wyller, and J. J. Rasmussen, Phys. Rev. E **66**, 046619 (2002).
[22] M. Peccianti, K. A. Brzdkiewicz, and G. Assanto, Opt. Lett. **27**, 1460 (2002).
[23] Z. Xu, Y. V. Kartashov, and L. Torner, Opt. Lett. **30**, 3171 (2005).
[24] Y. Y. Lin, R.-K. Lee, and B. A. Malomed, Phys. Rev. A **80**, 013838 (2009).
[25] Y. Y. Lin and R.-K. Lee, Opt. Express **15**, 8781 (2007).
[26] G. C. Duree, J. L. Shultz, G. J. Salamo, M. Segev, A. Yariv, B. Crosignani, P. DiPorto, E. J. Sharp, and R. R. Neurgaonkar, Phys. Rev. Lett. **71**, 533 (1993).
[27] C. Conti, M. Peccianti, and G. Assanto, Phys. Rev. Lett. **91**, 073901 (2003).
[28] C. Rotschild, O. Cohen, O. Manela, M. Segev, and T. Carmon, Phys. Rev. Lett. **95**, 213904 (2005).
[29] N. K. Efremidis, Phys. Rev. A **77**, 063824 (2008).
[30] H. Sakaguchi and B. A. Malomed, Phys. Rev. A **81**, 013624 (2010).
[31] T. J. Alexander, E. A. Ostrovskaya, and Yu. S. Kivshar, Phys. Rev. Lett. **96**, 040401 (2006).
[32] B. Eiermann, T. Anker, M. Albiez, M. Taglieber, P. Treutlein, K. P. Marzlin, and M. K. Oberthaler, Phys. Rev. Lett. **92**, 230401 (2004).
[33] A. Griesmaier, J. Werner, S. Hensler, J. Stuhler, and T. Pfau, Phys. Rev. Lett. **94**, 160401 (2005).
[34] J. Werner, A. Griesmaier, S. Hensler, J. Stuhler, T. Pfau, A. Simoni, and E. Tiesinga, Phys. Rev. Lett. **94**, 183201 (2005).
[35] J. Stuhler, A. Griesmaier, T. Koch, M. Fattori, T. Pfau, S. Giovanazzi, P. Pedri, and L. Santos, Phys. Rev. Lett. **95**, 150406 (2005).
[36] A. Griesmaier, J. Stuhler, and T. Pfau, Appl. Phys. B **82**, 211 (2006).
[37] Q. Beaufils, R. Chicireanu, T. Zanon, B. Laburthe-Tolra, E. Maréchal, L. Vernac, J.-C. Keller, and O. Gorceix, Phys. Rev. A **77**, 061601(R) (2008).
[38] T. Lahaye, C. Menotti, L. Santos, M. Lewenstein, and T. Pfau, Rep. Prog. Phys. **72**, 12640 (2009).
[39] Y. Y. Lin, R.-K. Lee, Y.-M. Kao, and T.-F. Jiang, Phys. Rev. A **78**, 023629 (2008).
[40] J. Cuevas, B. A. Malomed, P. G. Kevrekidis, and D. J. Frantzeskakis, Phys. Rev. A **79**, 053608 (2009).
[41] P. J. Y. Louis, E. A. Ostrovskaya, C. M. Savage, and Yu. S. Kivshar, Phys. Rev. A **67**, 013602 (2003).
[42] V. Prytula, V. Vekslerchik, and V. M. Pérez-García, Phys. Rev. E **78**, 027601 (2008).